Science Advances
AAAS

Supplementary Materials for

Krüppel-like factor 4 regulates the cytolytic effector function of exhausted CD8 T cells

Jinwoo Nah and Rho H. Seong

Corresponding author: Rho H. Seong, rhseong@snu.ac.kr

Sci. Adv. **8**, eadc9346 (2022)
DOI: 10.1126/sciadv.adc9346

This PDF file includes:

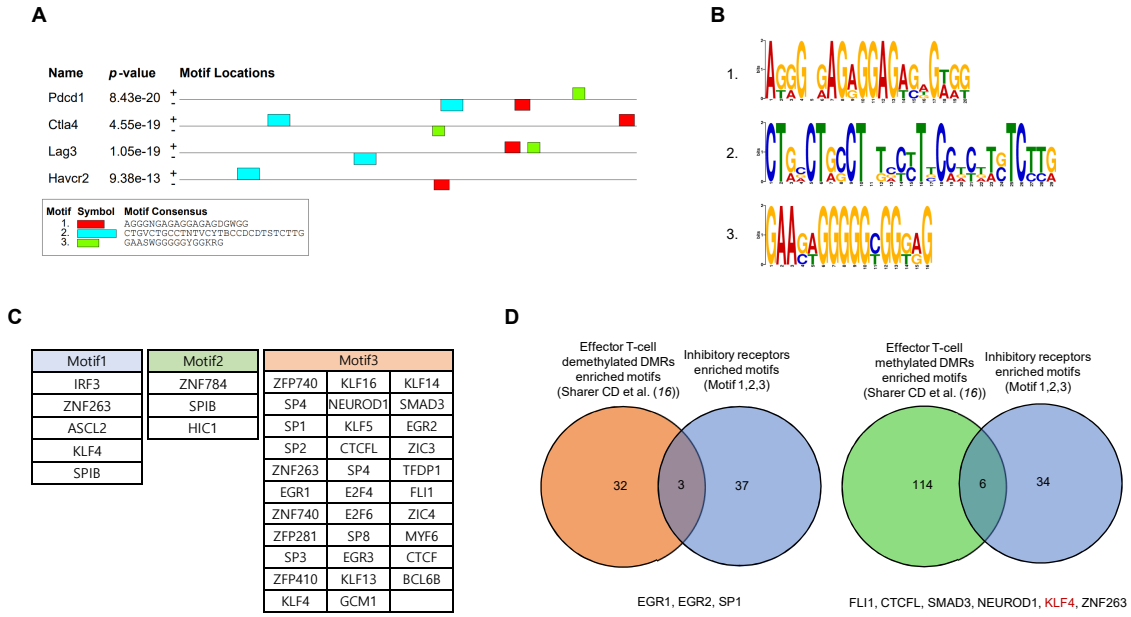

Fig. S1. KLF4 is a potential regulator of CD8 T-cell effector function during the exhaustion process. (**A**–**C**) Consensus motifs within *Pdcd1, Ctla4, Lag3,* and *Havcr2* promoter regions were analyzed using the MEME suite. (**A**) Location of 3 consensus motifs within the inhibitory receptor genes. (**B**) Sequences of 3 consensus motifs. (**C**) Analysis of binding targets on 3 consensus motifs using Tomtom Analysis. (**D**) Venn diagram comparing the list of binding targets on motifs related to CD8 T-cell effector differentiation (Sharer CD et al. (*16*)) and exhaustion (Motif 1, 2, 3).

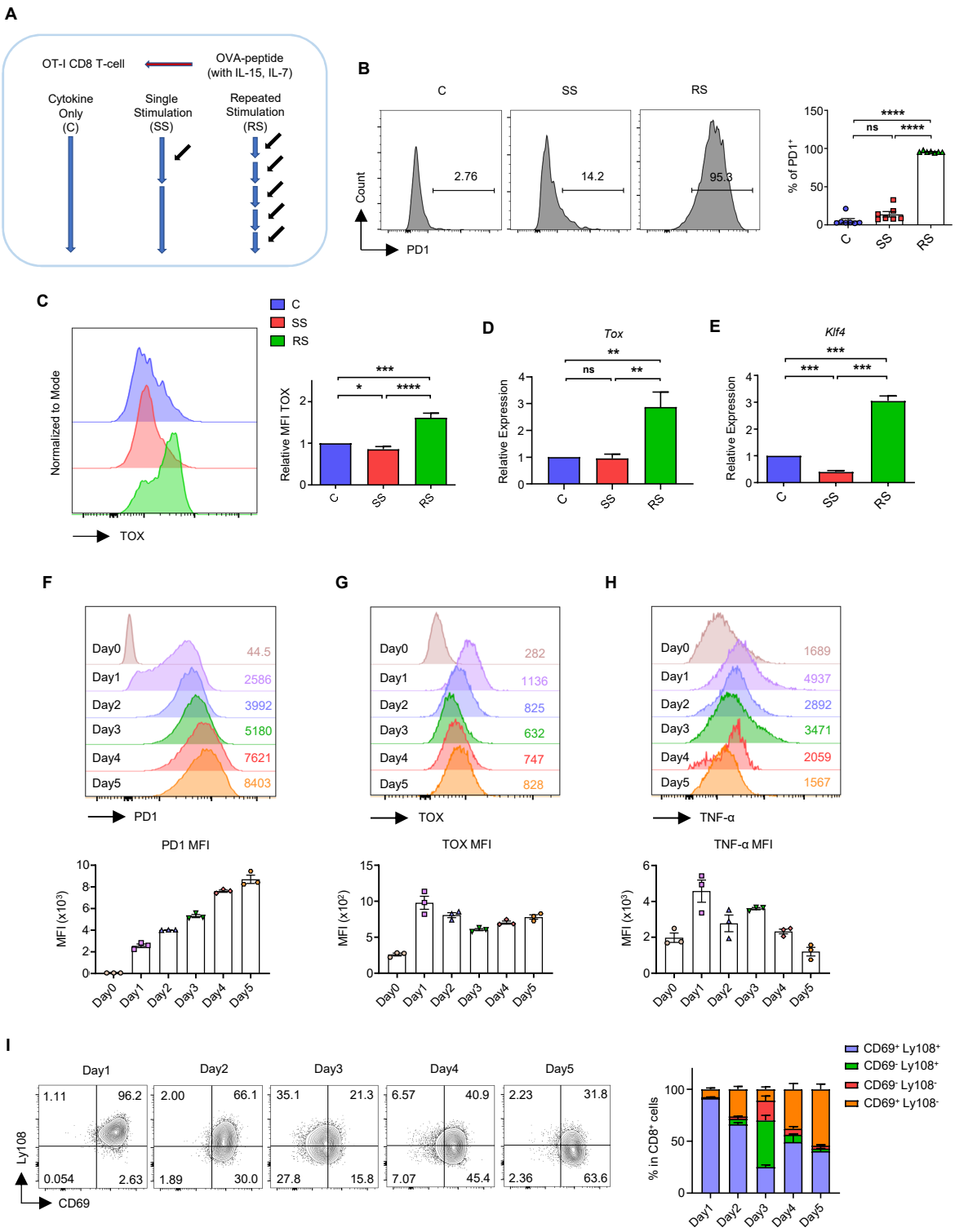
A
OT-I CD8 T-cell
OVA-peptide
(with IL-15, IL-7)
Cytokine
Only
(C)
Single
Stimulation
(SS)
Repeated
Stimulation
(RS)
B
C
SS
RS
Count
2.76
14.2
95.3
PD1
% of PD1+
ns
****
C
C
SS
RS
Normalized to Mode
TOX
Relative MFI TOX
*
***
****
D
Tox
Relative Expression
ns
**
E
Klf4
***
F
Day0
Day1
Day2
Day3
Day4
Day5
44.5
2586
3992
5180
7621
8403
PD1
PD1 MFI
MFI (x10³)
G
282
1136
825
632
747
828
TOX
TOX MFI
MFI (x10²)
H
1689
4937
2892
3471
2059
1567
TNF-α
TNF-α MFI
MFI (x10³)
I
Day1
Day2
Day3
Day4
Day5
Ly108
CD69
1.11
96.2
0.054
2.63
2.00
66.1
1.89
30.0
35.1
21.3
27.8
15.8
6.57
40.9
7.07
45.4
2.23
31.8
2.36
63.6
CD69+ Ly108+
CD69- Ly108+
CD69- Ly108-
CD69+ Ly108-
% in CD8+ cells

Fig. S2. *Klf4* is increased by chronic TCR stimulation-induced exhaustion. (A-E) Naïve OT-I CD8 T-cells were isolated and cultured under 3 different conditions; cytokine only (C), single stimulation (SS), and repeated stimulation (RS) cells. (**A**) Schematic design of the *in vitro* exhaustion experiment. (**B**) Representative flow cytometry plot of PD1 expression and the proportion of $PD1^+$ cells in each group (n=7 per group). (**C**) Representative flow cytometry plot of TOX expression and histogram of relative TOX MFI level in each group (n=7 per group). (**D**) Histogram of *Tox* mRNA expression in each group (n=7 per group). (**E**) Histogram of *Klf4* mRNA expression in each group (n=7 per group). (**F-I**) Naïve OT-I CD8 T-cells were isolated and repeatedly stimulated by OVA peptide. Flow cytometry analysis was performed daily. (**F**) Representative flow cytometry plot and histogram of PD1 MFI on Day0~Day5 (n=3 per group). (**G**) Representative flow cytometry plot and histogram of TOX MFI on Day0~Day5 (n=3 per group). (**H**) Representative flow cytometry plot and histogram of TNF-α MFI on Day0~Day5 (n=3 per group). (**I**) Representative flow cytometry plot of CD69 and Ly108 expression, and histogram of the CD69-Ly108 subset proportion on Day1~Day5 (n=7 per group). All data are mean±SEM. Statistical analysis was performed using Student's *t*-test. ns (non-significant, $P > 0.05$); * $P < 0.05$; ** $P < 0.01$; *** $P < 0.001$; **** $P < 0.0001$.

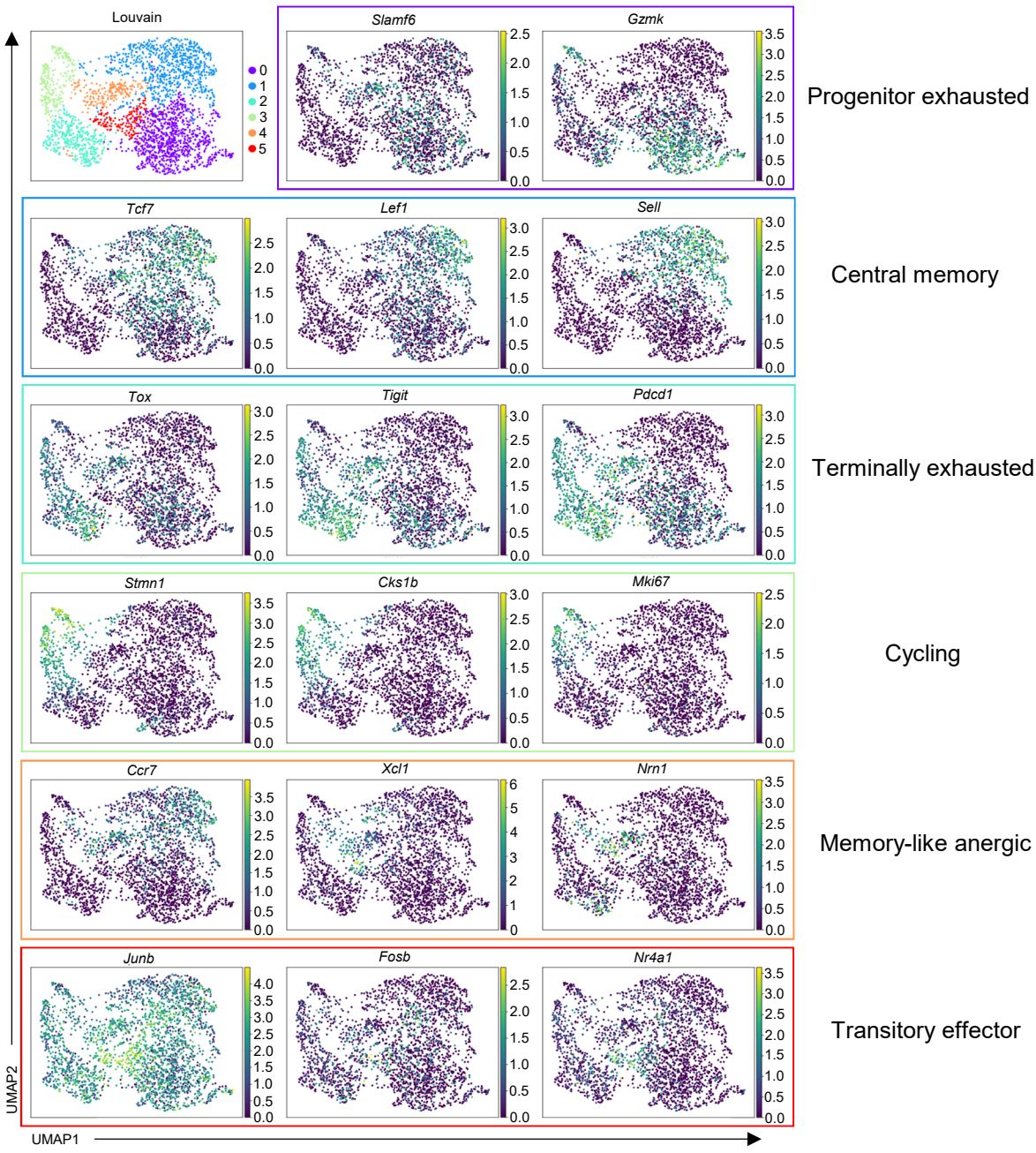

Fig. S3. Clustering, UMAP visualization of functional annotating genes on *Pdcd1*-expressing CD8⁺ TILs. Single-cell RNA-sequencing data from B16F10 melanoma infiltrating CD8⁺ TILs (GSE116390) were analyzed. *Pdcd1*-expressing CD8⁺ TILs were filtered. Clustering and UMAP visualization of progenitor exhausted subset signature (*Slamf6, Gzmk*), central memory signature (*Tcf7, Lef1, Sell*), terminally exhausted subset signature (*Tox, Tigit, Pdcd1*), cycling signature (*Stmn1, Cks1b, Mki67*), memory-like anergic signature (*Ccr7, Xcl1, Nrn1*), transitory effector signature (*Junb, Fosb, Nr4a1*). Clustered by Louvain method.

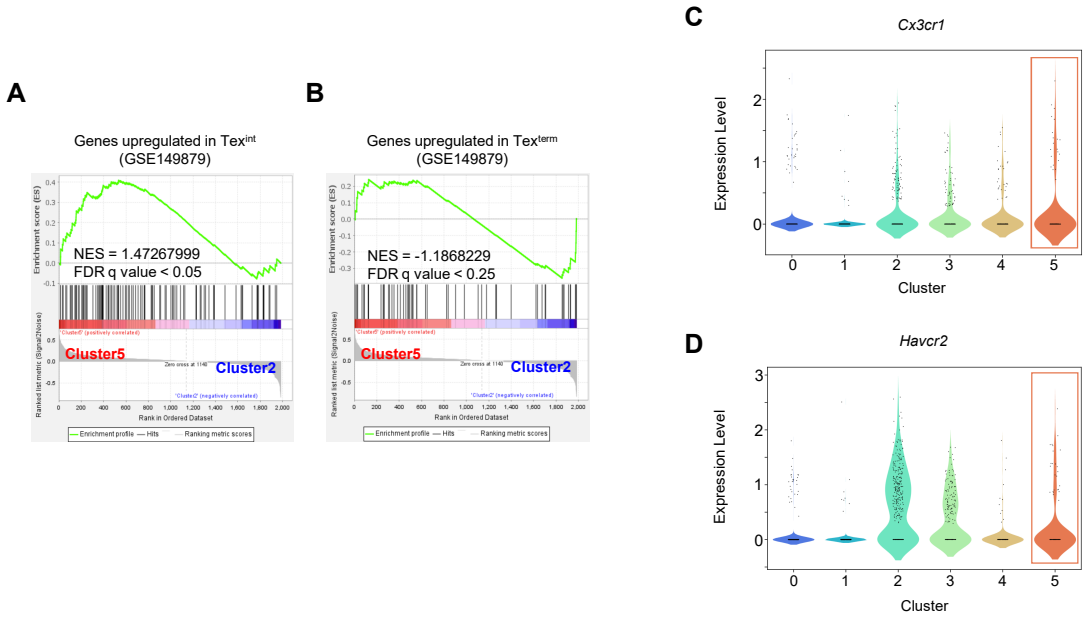

Fig. S4. Cluster 5 cells show the characteristics of transitory/intermediate exhausted CD8 T-cells. (**A-B**) Gene set enrichment analysis (GSEA) between cluster 2 and cluster 5 cells using gene sets of (**A**) genes upregulated in Tex^{int} (GSE149879) and (**B**) genes upregulated in Tex^{term} (GSE149879). (**C**) Violin plot of the expression level of *Cx3cr1* within clusters. (**D**) Violin plot of the expression level of *Havcr2* within clusters. Cluster 5 denotes transitory effector cells.

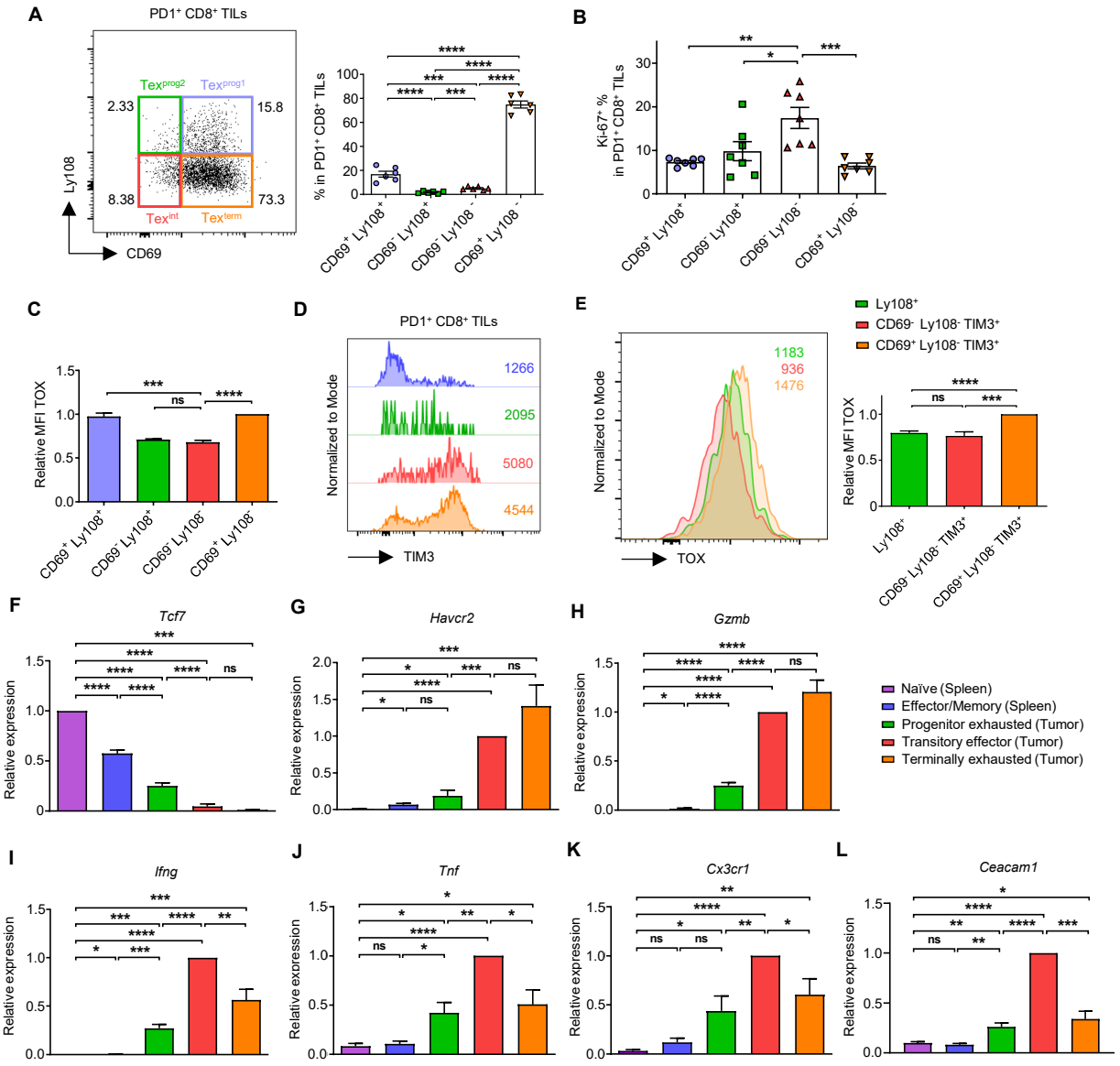

Fig. S5. Profiles and characteristics of exhausted CD8 T-cell populations. (**A-E**) CD8$^+$ TILs were analyzed from MC38 tumor bearing C57BL/6 mice on day18. (**A**) Representative flow cytometry plot of CD69 and Ly108 expression and the proportion of subpopulations (Tex^{prog1}, Tex^{prog2}, Tex^{int}, and Tex^{term}) (n=6 per group) in PD1$^+$CD8$^+$ TILs. (**B**) The proportion of Ki-67$^+$ cells in PD1$^+$CD8$^+$ TIL subpopulations (n=7 per group). (**C**) Histogram of the relative TOX MFI (Mean Fluorescence Intensity) in PD1$^+$CD8$^+$ TIL subpopulations (n=4 per group). (**D**) Representative flow cytometry plot of TIM3 expression in PD1$^+$CD8$^+$ TILs subpopulations. (**E**) Representative flow cytometry plot of TOX expression and histogram of the relative TOX MFI in 3 different PD1$^+$CD8$^+$ TIL subpopulations (n=5 per group). (**F-L**) CD8 T-cell subpopulations of spleen and tumor from MC38 tumor bearing C57BL/6 mice were isolated and their gene expression were analyzed. Histogram of (**F**) *Tcf7* (n=8 per group), (**G**) *Havcr2* (n=7 per group), (**H**) *Gzmb* (n=9 per group), (**I**) *Ifng* (n=5 per group), (**J**) *Tnf* (n=3 per group), (**K**) *Cx3cr1* (n=8 per group), (**L**) *Ceacam1* (n=4 per group) mRNA expression in CD8 T-cell subpopulations. All data are mean±SEM. Statistical analysis was performed using Student's *t*-test. ns (non-significant, P > 0.05); * P < 0.05; ** P < 0.01; *** P < 0.001; **** P < 0.0001.

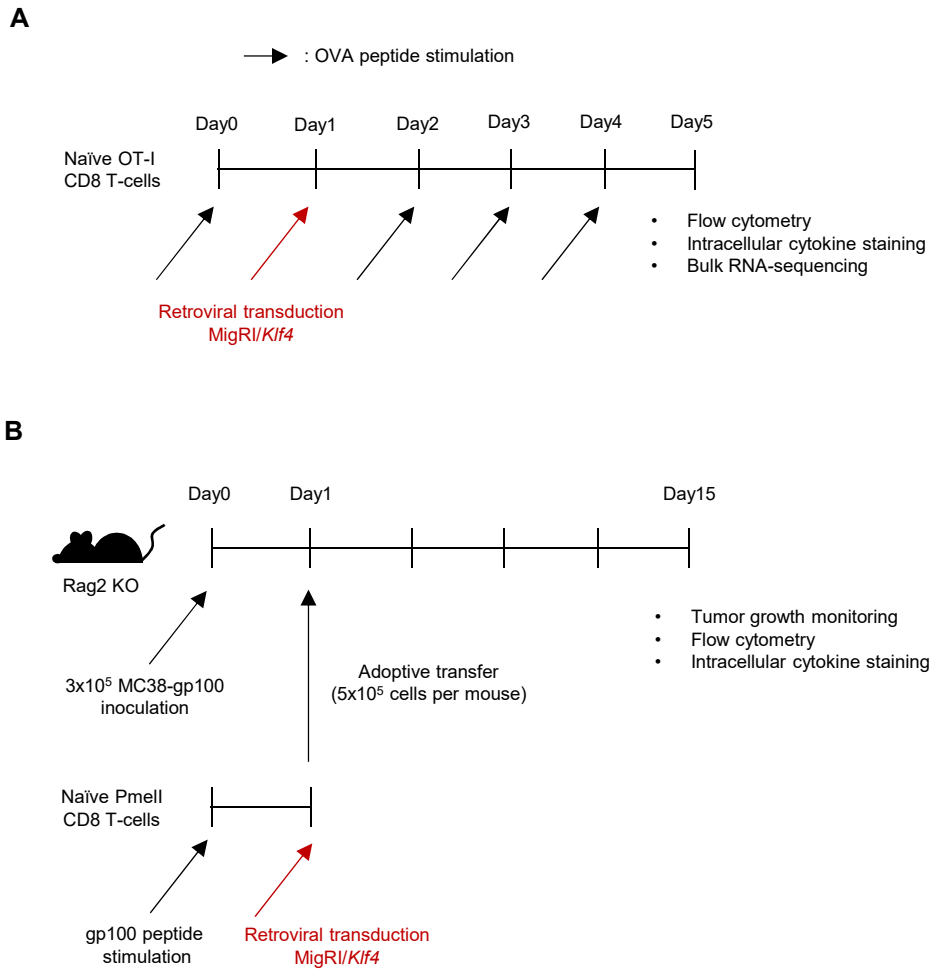

Fig. S6. Schematic designs of *Klf4* overexpression in *in vitro* and *in vivo* experiments. (**A**) Schematic design of *Klf4* overexpression in the *in vitro* exhaustion model. Naïve OT-I CD8 T-cells were isolated and stimulated with OVA peptide for 24hrs. Then the cells were retrovirally transduced with MigRI/*Klf4* and repeatedly stimulated with OVA peptide until day5. On day5, transduced cells were analyzed by flow cytometry and bulk RNA-sequencing. (**B**) Schematic design of *Klf4* overexpression in the *in vivo* mouse experiment. $3x10^5$ MC38-gp100 cells were subcutaneously injected into the right flank of Rag2 KO mice. At the same time, naïve PmelI CD8 T-cells were isolated and stimulated with gp100 peptides for 24hrs. A day after the tumor cell injection, activated PmelI CD8 T-cells were retrovirally transduced with MigRI/*Klf4* and $5x10^5$ cells were adoptive transferred into the tumor inoculated mice. Tumor growth was monitored and phenotypes of tumor-infiltrating CD8 T-cells were analyzed by flow cytometry on day15.

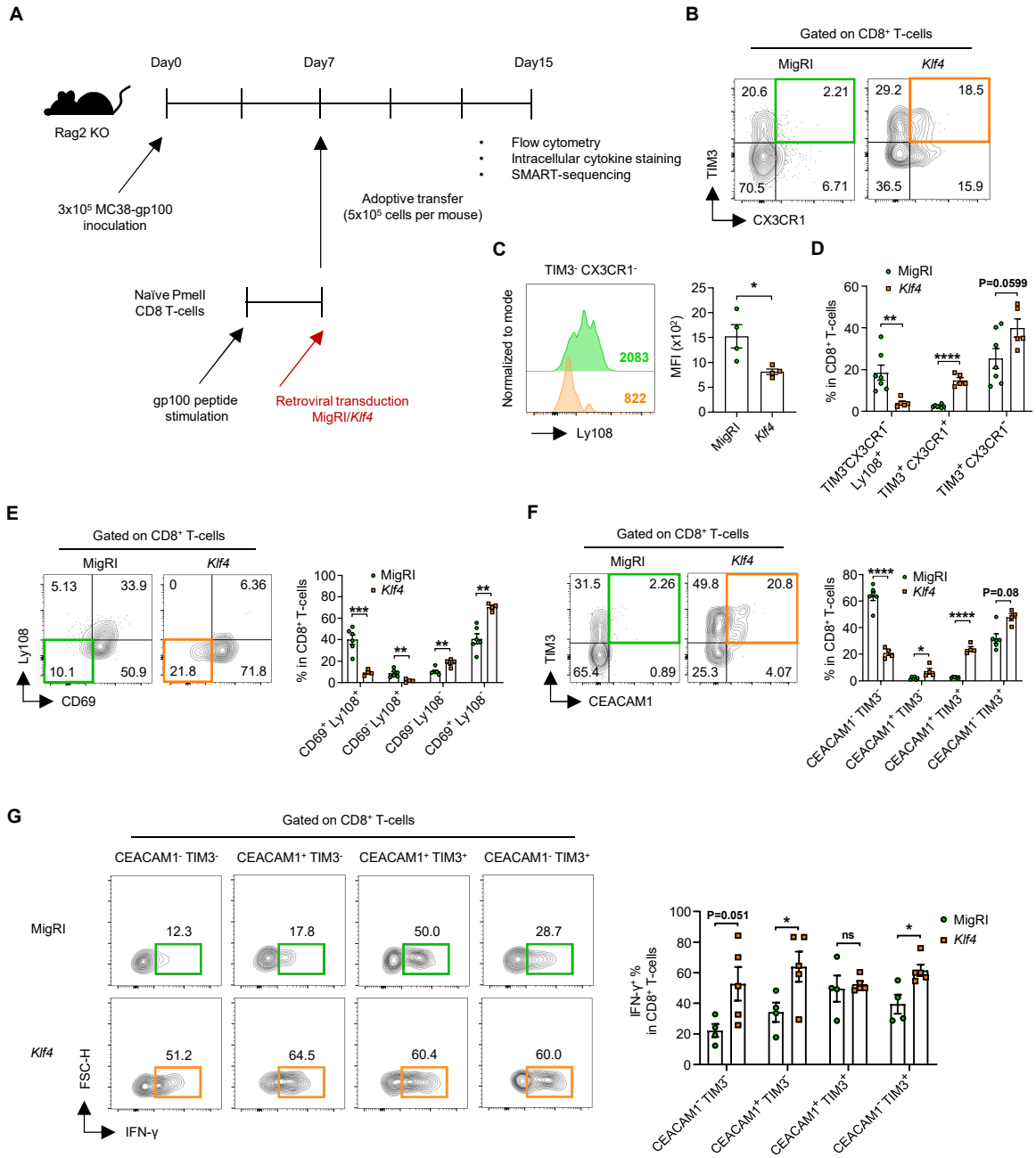
A
Day0
Day7
Day15
Rag2 KO
3x10⁵ MC38-gp100 inoculation
Adoptive transfer (5x10⁵ cells per mouse)
Flow cytometry
Intracellular cytokine staining
SMART-sequencing
Naïve PmelI CD8 T-cells
gp100 peptide stimulation
Retroviral transduction MigRI/Klf4
B
Gated on CD8⁺ T-cells
MigRI
Klf4
20.6
2.21
70.5
6.71
29.2
18.5
36.5
15.9
TIM3
CX3CR1
C
TIM3⁻ CX3CR1⁻
Normalized to mode
2083
822
Ly108
MFI (x10²)
MigRI
Klf4
D
MigRI
Klf4
% in CD8⁺ T-cells
P=0.0599
TIM3⁻CX3CR1⁻ Ly108⁺
TIM3⁺ CX3CR1⁺
TIM3⁺ CX3CR1⁻
E
Gated on CD8⁺ T-cells
MigRI
Klf4
5.13
33.9
10.1
50.9
0
6.36
21.8
71.8
Ly108
CD69
% in CD8⁺ T-cells
CD69⁺ Ly108⁺
CD69⁻ Ly108⁺
CD69⁺ Ly108⁻
CD69⁻ Ly108⁻
F
Gated on CD8⁺ T-cells
MigRI
Klf4
31.5
2.26
65.4
0.89
49.8
20.8
25.3
4.07
TIM3
CEACAM1
% in CD8⁺ T-cells
P=0.08
CEACAM1⁻TIM3⁻
CEACAM1⁺ TIM3⁻
CEACAM1⁺ TIM3⁺
CEACAM1⁻ TIM3⁺
G
Gated on CD8⁺ T-cells
CEACAM1⁻ TIM3⁻
CEACAM1⁺ TIM3⁻
CEACAM1⁺ TIM3⁺
CEACAM1⁻ TIM3⁺
MigRI
Klf4
12.3
17.8
50.0
28.7
51.2
64.5
60.4
60.0
FSC-H
IFN-γ
IFN-γ⁺ % in CD8⁺ T-cells
P=0.051
ns
MigRI
Klf4
CEACAM1⁻TIM3⁻
CEACAM1⁺ TIM3⁻
CEACAM1⁺ TIM3⁺
CEACAM1⁻TIM3⁺

Fig. S7. KLF4 overexpression promotes the generation of transitory/intermediate exhausted CD8 T-cells and enhances their effector function. (**A**-**G**) $3x10^5$ MC38-gp100 cells were subcutaneously injected into the right flank of Rag2 KO mice. $5x10^5$ CD8 T-cells transduced with MigRI/*Klf4* were adoptive transferred into the tumor inoculated mice on day7. Tumor-infiltrating CD8 T-cells were analyzed on day15. GFP^+ cells were gated for all analyses. (**A**) Schematic design of *Klf4* overexpression in the *in vivo* mouse experiment. (**B**) Representative flow cytometry plot of CX3CR1 and TIM3 expression in CD8 T-cells transduced with MigRI/*Klf4*. (**C**) Representative flow cytometry plot of Ly108 expression, and histogram of Ly108 MFI in $TIM3^-CX3CR1^-$ CD8 T-cells transduced with MigRI/*Klf4* (n=4 per group). (**D**) The proportion of progenitor exhausted ($TIM3^-CX3CR1^-Ly108^+$), transitory ($TIM3^+CX3CR1^+$), and terminally exhausted ($TIM3^+CX3CR1^-$) subsets in CD8 T-cells transduced with MigRI(n=7)/*Klf4*(n=5). (**E**) Representative flow cytometry plot of CD69 and Ly108 expression, and the proportion of Tex^{prog1} ($CD69^+Ly108^+$), Tex^{prog2} ($CD69^-Ly108^+$), Tex^{int} ($CD69^-Ly108^-$), and Tex^{term} ($CD69^+Ly108^-$) in CD8 T-cells transduced with MigRI(n=6)/*Klf4*(n=4). (**F**) Representative flow cytometry plot of CEACAM1 and TIM3 expression, and the proportion of CEACAM1-TIM3 defined subsets in CD8 T-cells transduced with MigRI(n=6)/*Klf4*(n=4). (**G**) Representative flow cytometry plot of IFN-γ expression and the proportion of IFN-γ^+ cells within CEACAM1-TIM3 defined CD8 T-cell subsets transduced with MigRI(n=4)/*Klf4*(n=5). All data are mean±SEM. Statistical analysis was performed using Student's *t*-test. ns (non-significant, $P > 0.05$); * $P < 0.05$; ** $P < 0.01$; *** $P < 0.001$; **** $P < 0.0001$.

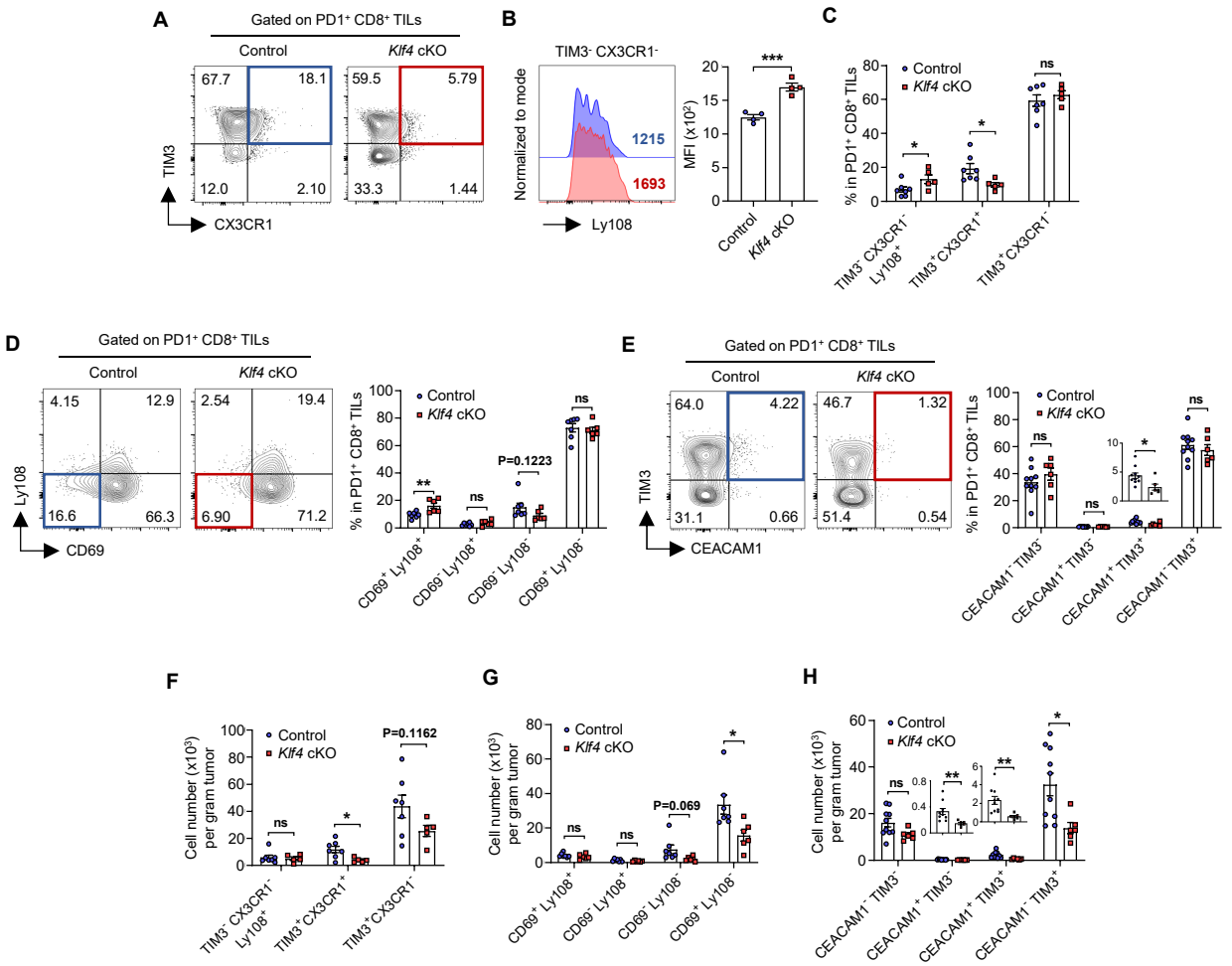

Fig. S8. *Klf4* deficiency impairs the generation of transitory/intermediate exhausted CD8 T-cells. (**A-H**) 3x10^5 MC38 cells were subcutaneously injected into the right flank of Control/*Klf4* cKO mice. CD8$^+$ TILs were analyzed on day14. (**A**) Representative flow cytometry plot of CX3CR1 and TIM3 expression in PD1$^+$CD8$^+$ TILs from Control/*Klf4* cKO mice. (**B**) Representative flow cytometry plot of Ly108 expression and histogram of Ly108 MFI in TIM3$^-$CX3CR1$^-$ PD1$^+$CD8$^+$ TILs from Control(n=4)/*Klf4* cKO(n=4) mice. (**C**) The proportion of progenitor exhausted (TIM3$^-$CX3CR1$^-$Ly108$^+$), transitory (TIM3$^+$CX3CR1$^+$), and terminally exhausted (TIM3$^+$CX3CR1$^-$) subsets in PD1$^+$CD8$^+$ TILs from Control(n=7)/*Klf4* cKO(n=5) mice. (**D**) Representative flow cytometry plot of CD69 and Ly108 expression, and the proportion of Tex^{prog1} (CD69$^+$Ly108$^+$), Tex^{prog2} (CD69$^-$Ly108$^+$), Tex^{int} (CD69$^-$ Ly108$^-$), and Tex^{term} (CD69$^+$Ly108$^-$) in PD1$^+$CD8$^+$ TILs from Control(n=7)/*Klf4* cKO(n=6) mice. (**E**) Representative flow cytometry plot of CEACAM1 and TIM3 expression, and the proportion of CEACAM1-TIM3 defined subsets in PD1$^+$CD8$^+$ TILs from Control(n=10)/*Klf4* cKO(n=6) mice. (**F-H**) The absolute cell number of (**F**) TIM3-CX3CR1-Ly108 defined subsets, (**G**) CD69-Ly108 defined subsets, and (**H**) CEACAM1-TIM3 defined subsets. All data are mean±SEM. Statistical analysis was performed using Student's *t*-test. ns (non-significant, P > 0.05); * P < 0.05; ** P < 0.01; *** P < 0.001; **** P < 0.0001.

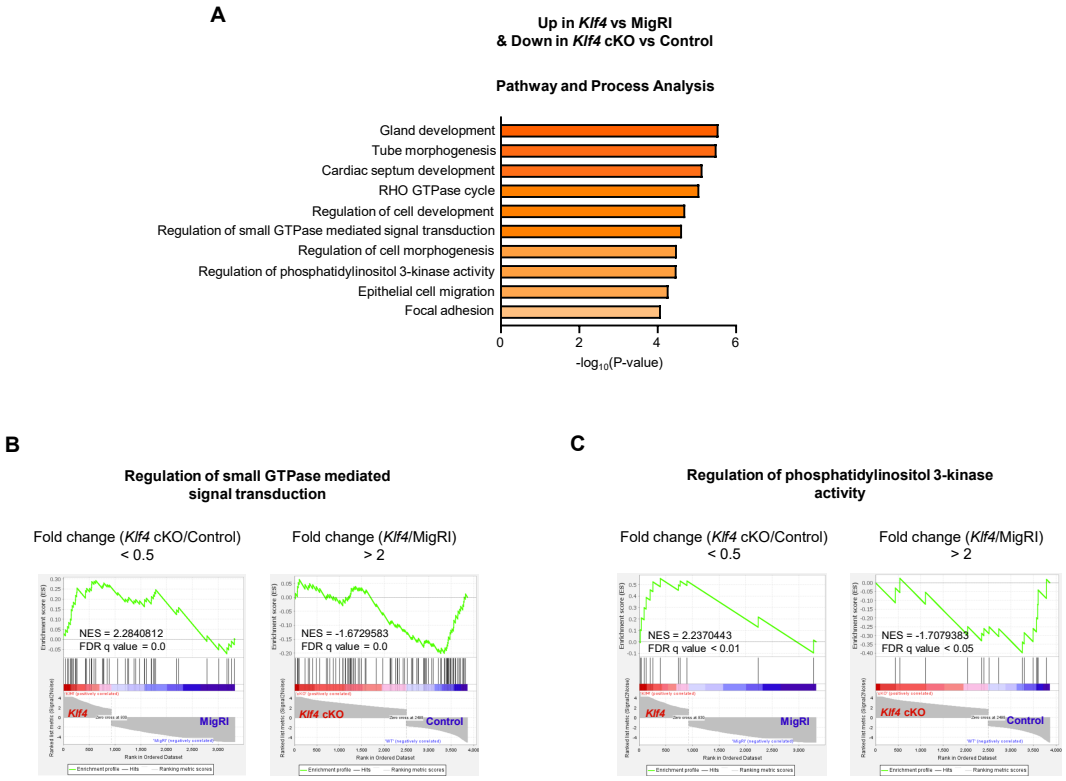

Fig. S9. KLF4 regulates small GTPase and PI3K mediated signaling pathway. (**A**) Gene ontology (Pathway and process) analysis of genes which are upregulated by *Klf4* overexpression and downregulated by *Klf4* deficiency at the same time. (**B-C**) Gene set enrichment analysis (GSEA) between CD8 T-cells transduced with MigRI/*Klf4* among the genes decreased by *Klf4* deficiency, and GSEA between Control/*Klf4* cKO PD1^{+}CD8^{+} TILs among the genes increased by *Klf4* overexpression, using gene sets of (**B**) regulation of small GTPase mediated signal transduction and (**C**) regulation of phosphatidylinositol 3-kinase (PI3K) activity.

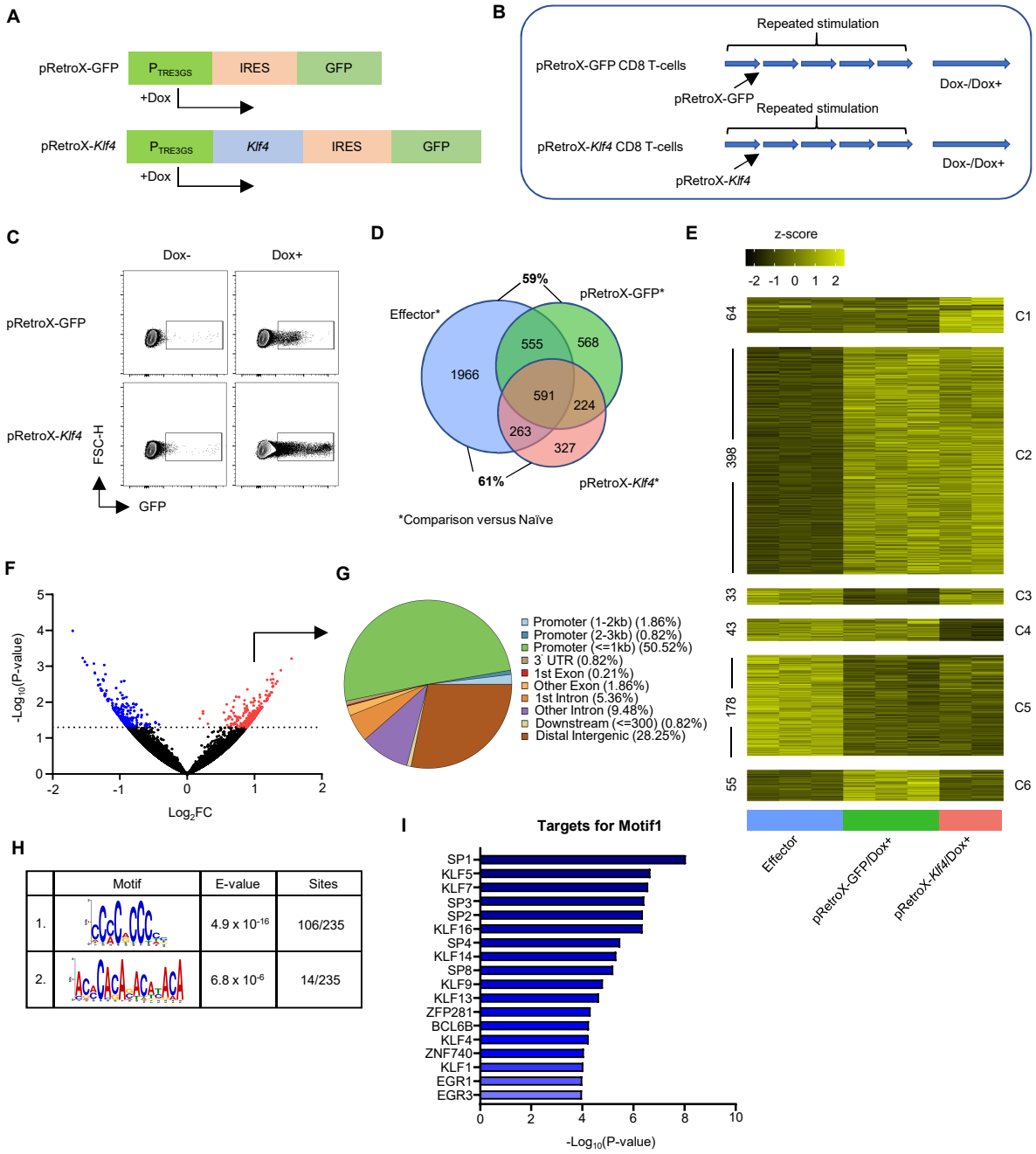
A
pRetroX-GFP
P TRE3GS
IRES
GFP
+Dox
pRetroX-Klf4
P TRE3GS
Klf4
IRES
GFP
+Dox
B
Repeated stimulation
pRetroX-GFP CD8 T-cells
pRetroX-GFP
Dox-/Dox+
Repeated stimulation
pRetroX-Klf4 CD8 T-cells
pRetroX-Klf4
Dox-/Dox+
C
Dox-
Dox+
pRetroX-GFP
pRetroX-Klf4
FSC-H
GFP
D
59%
pRetroX-GFP*
Effector*
555
568
1966
591
224
263
327
61%
pRetroX-Klf4*
*Comparison versus Naïve
E
z-score
-2 -1 0 1 2
64
C1
398
C2
33
C3
43
C4
178
C5
55
C6
Effector
pRetroX-GFP/Dox+
pRetroX-Klf4/Dox+
F
-Log10(P-value)
Log2FC
G
Promoter (1-2kb) (1.86%)
Promoter (2-3kb) (0.82%)
Promoter (<=1kb) (50.52%)
3' UTR (0.82%)
1st Exon (0.21%)
Other Exon (1.86%)
1st Intron (5.36%)
Other Intron (9.48%)
Downstream (<=300) (0.82%)
Distal Intergenic (28.25%)
H
Motif
E-value
Sites
1.
4.9 x 10-16
106/235
2.
6.8 x 10-6
14/235
I
Targets for Motif1
SP1
KLF5
KLF7
SP3
SP2
KLF16
SP4
KLF14
SP8
KLF9
KLF13
ZFP281
BCL6B
KLF4
ZNF740
KLF1
EGR1
EGR3
-Log10(P-value)

Fig. S10. Induction of *Klf4* on exhausted CD8 T-cells using Retro-X Tet-One system and analyses of ATAC-sequencing. (**A**) Schematic design of pRetroX-GFP and pRetoX-*Klf4* vector construct. (**B**-**C**) OT-I CD8 T-cells were transduced with pRetroX-GFP/pRteroX-*Klf4* at day1 during *in vitro* exhaustion process. Exhausted CD8 T-cells were harvested on day5 and cultured with or without doxycycline for additional 2 days. (**B**) Schematic design of the experiment. (**C**) Representative flow cytometry plot of GFP expression in each group. (**D**-**I**) ATAC-sequencing analysis on naïve, effector, pRetroX-GFP/Dox+, and pRetroX-*Klf4*/Dox+ CD8 T-cells was performed. Effector cells were *in vitro* generated by peptide stimulation for 2 days. (**D**) Venn diagram for DARs (Differentially Accessible Regions) of effector, pRetroX-GFP/Dox+, and pRetroX-*Klf4*/Dox+ CD8 T-cells compared to naïve CD8 T-cells. (**E**) Heat map of differential peaks corresponding to DARs significantly different between effector, pRetroX-GFP/Dox+, and pRetroX-*Klf4*/Dox+ CD8 T-cells. Calculated by pairwise DEseq2 analysis. (**F**) Volcano plot of DARs between pRetroX-GFP/Dox+ and pRetroX-*Klf4*/Dox+ CD8 T-cells. (**G**) Genome location of more accessible DARs on pRetroX-*Klf4*/Dox+ CD8 T-cells compared to pRetroX-GFP/Dox+ CD8 T-cells. Analyzed by ChIPseeker. (**H**) Enriched motifs in more accessible DARs on pRetroX-*Klf4*/Dox+ CD8 T-cells compared to pRetroX-GFP/Dox+ CD8 T-cells. Calculated by MEME-ChIP. (**I**) Potential transcription factors binding Motif1. Calculated by Tomtom analysis.

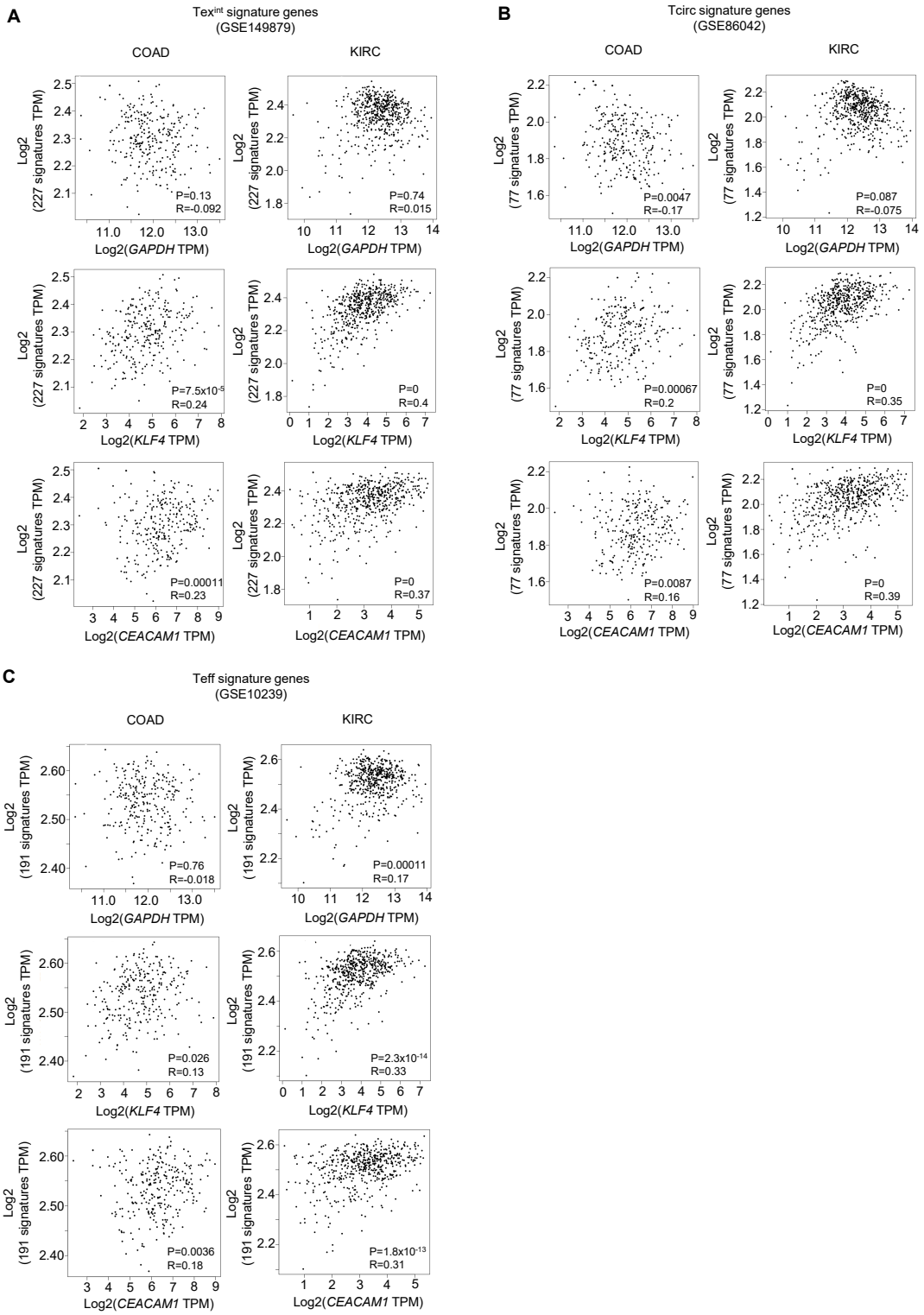

Fig. S11. *KLF4* expression shows a positive correlation with effector CD8 T-cell signatures in human cancer patients. (**A**-**C**) Pearson-correlation between the gene expression of *GAPDH/KLF4/CEACAM1* and average expression of (**A**) Tex^{int} signature genes, (**B**) Tcirc signature genes, and (**C**) Teff signature genes in colon adenocarcinoma (COAD) and kidney renal clear cell carcinoma (KIRC) cancer patients. P-values less than 0.05 were considered to be significant by the Pearson-correlation test.

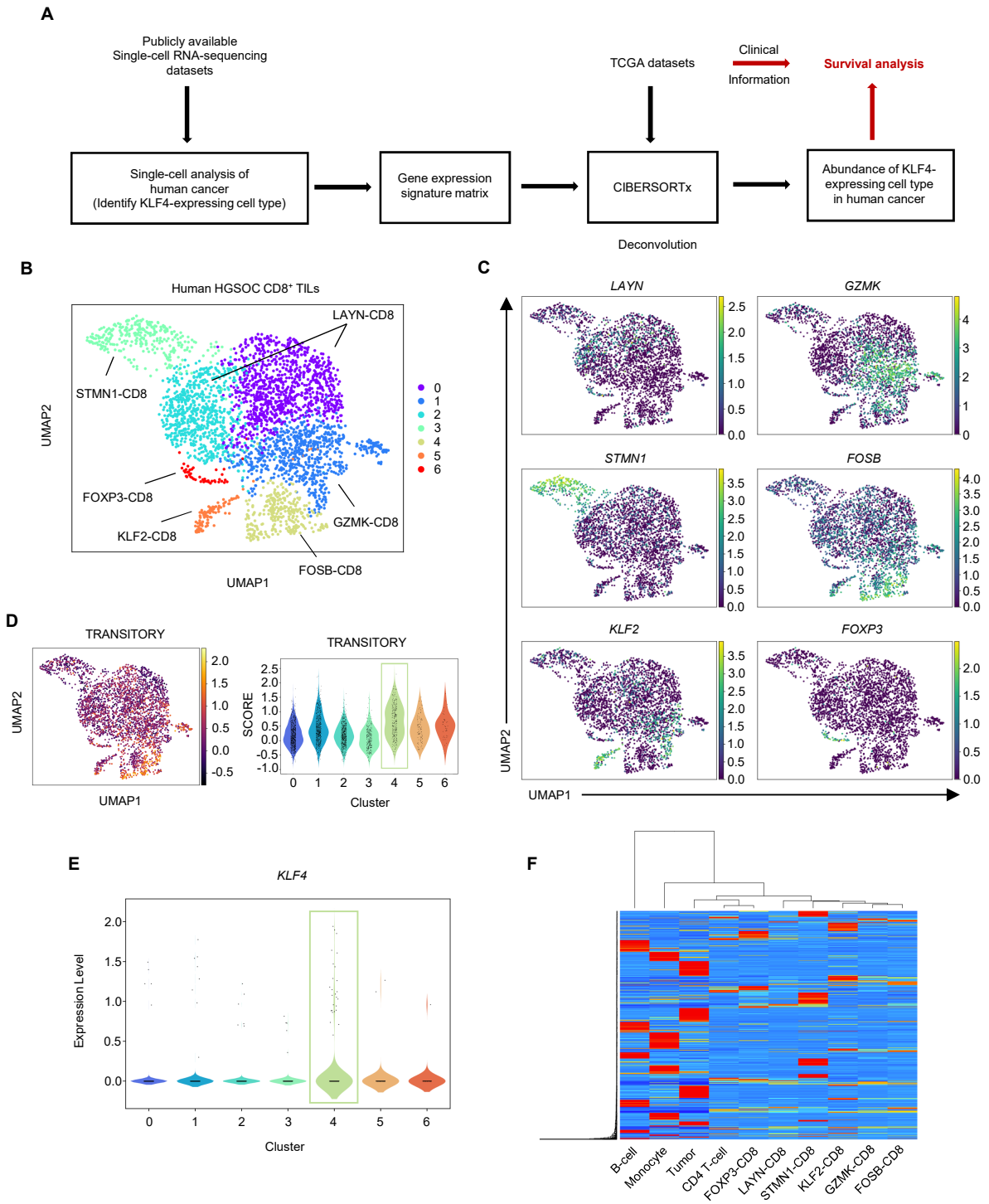

Fig. S12. Human counterparts of the mouse transitory effector subsets in cancer and generation of their signature matrix using CIBERSORTx. (**A**) Schematic design of cancer patient survival analysis using abundances of KLF4-expressing human transitory effector counterparts. (**B-E**) Single-cell RNA-sequencing data from high grade serous ovarian cancer (HGSOC) patients (GSE184880) were analyzed. CD8$^+$ TILs were filtered. (**B**) Clustering and UMAP visualization of CD8$^+$ TILs (n=3,137 cells). Colors denote transcriptional clusters, labeled with functional annotations. (**C**) UMAP visualization of *LAYN*, *GZMK*, *STMN1*, *FOSB*, *KLF2*, and *FOXP3.* Clustered by Louvain method. (**D**) UMAP visualization and violin plot of TRANSITORY signature score within CD8$^+$ TILs. (**E**) Violin plot of *KLF4* expression within clusters. (**F**) The signature matrix of 10 subsets including FOXP3-CD8, LAYN-CD8, STMN1-CD8, KLF2-CD8, GZMK-CD8, FOSB-CD8, as well as B-cell, monocyte, CD4 T-cell, and tumor cell. Performed by CIBERSORTx.

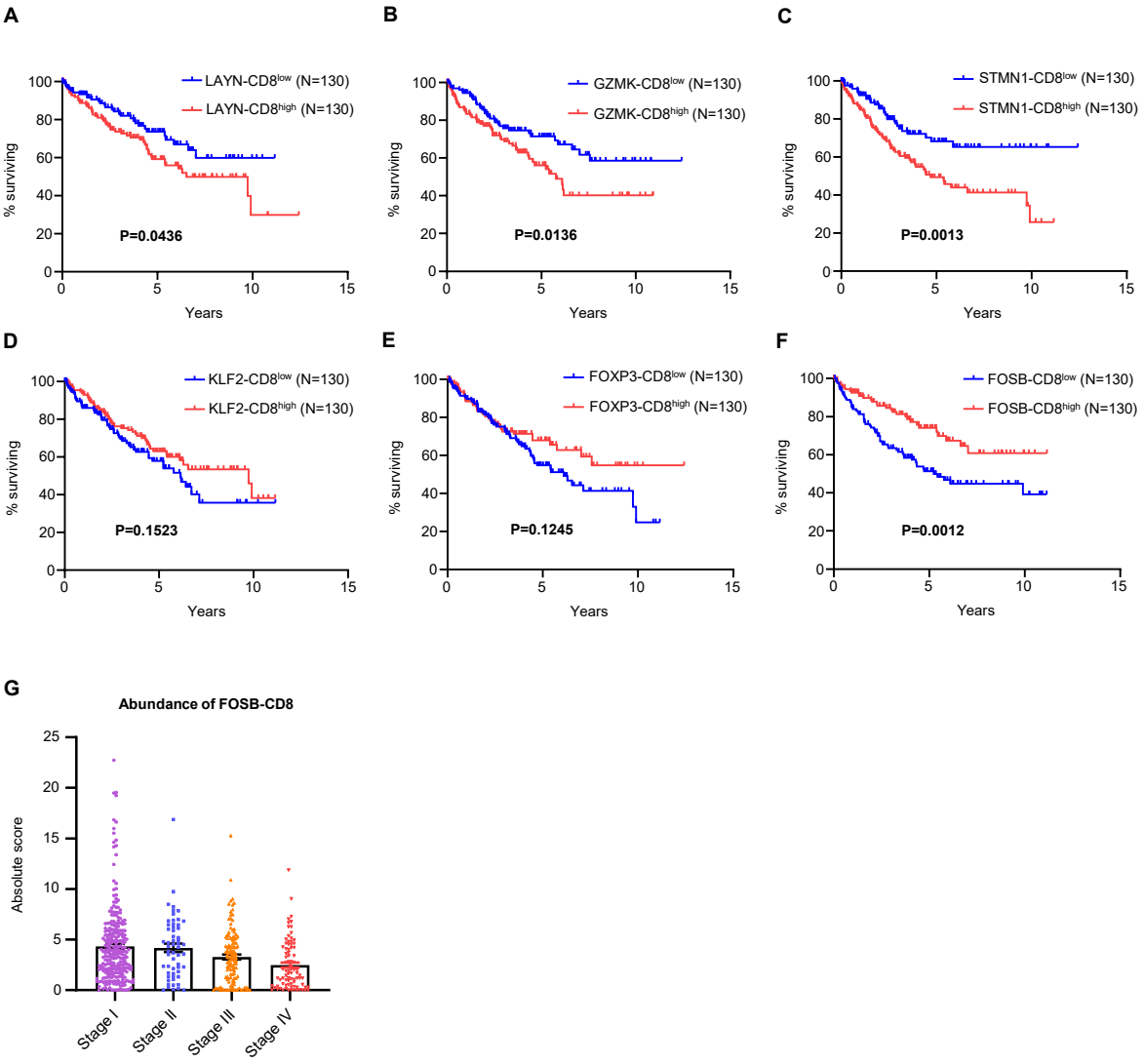

Fig. S13. Abundance of FOSB-CD8 T-cells correlates with a favorable tumor prognosis in KIRC patients. (**A-G**) Abundances of LAYN-CD8, GZMK-CD8, STMN1-CD8, KLF2-CD8, FOXP3-CD8, and FOSB-CD8 were calculated by CIBERSORTx and used for survival analysis in kidney renal clear cell carcinoma (KIRC) patients. Kaplan–Meier curve of KIRC patients based on the abundance (upper 25% and lower 25%) of (**A**) LAYN-CD8, (**B**) GZMK-CD8, (**C**) STMN1-CD8, (**D**) KLF2-CD8, (**E**) FOXP3-CD8, and (**F**) FOSB-CD8. (**G**) Abundance of FOSB-CD8 in patients with different prognostic stages (Stage I-IV).

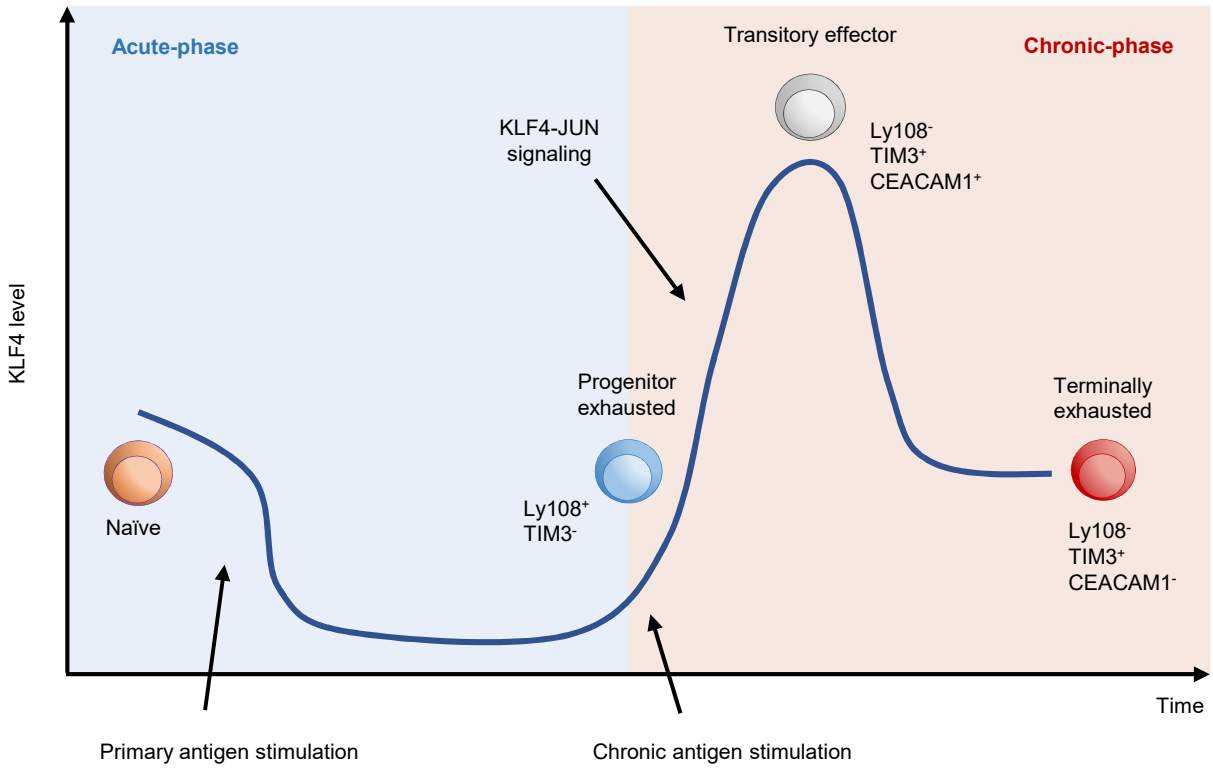

Fig. S14. KLF4 is a hallmark of cytolytic transitory effector CD8 T-cell during the exhaustion process. Schematic model highlighting the role of KLF4 in CD8 T-cells during the exhaustion process. In the acute phase, KLF4 expression is decreased by primary antigen stimulation. However, KLF4 expression is upregulated by chronic antigen stimulation. Increased KLF4 expression activates CD8 T-cell differentiation into cytolytic transitory effector subsets and their effector function, in part by enhancing c-Jun activity. KLF4-expressing transitory effector CD8 T-cells highly express CEACAM1 and TIM3, while terminally exhausted CD8 T-cells lose their KLF4 expression and downregulate CEACAM1. High KLF4 expression is required for maintaining the cytolytic function of transitory effector CD8 T-cells during the exhaustion process. The potential effects of KLF4 on CD8 T-cell exhaustion can be highlighted in terms of anti-tumor immune therapy.

#Primers for qRT-PCR	
Actb Forward	CGTGAAAAGATGACCCAGATCA
Actb Reverse	TGGTACGACCAGAGGCATACAG
Klf4 Forward	GTGCCCCGACTAACCGTTG
Klf4 Reverse	GTCGTTGAACTCCTCGGTCT
Tbx21 Forward	AGCAAGGACGGCGAATGTT
Tbx21 Reverse	GGGTGGACATATAAGCGGTTC
Eomes Forward	CGTTCACCCAGAATCTCCTAACA
Eomes Reverse	TGCAGCCTCGGTTGGTATTT
Tcf7 Forward	AGCTTTCTCCACTCTACGAACA
Tcf7 Reverse	AATCCAGAGAGATCGGGGGTC
Tox Forward	CAACTCAAAGCCGTCAGTATTCC
Tox Reverse	GCTGAGGAGTCATTCCTGGTT
Cx3cr1 Forward	GAGTATGACGATTCTGCTGAGG
Cx3cr1 Reverse	CAGACCGAACGTGAAGACGAG
Ifng Forward	GATGCATTCATGAGTATTGCCAAGT
Ifng Reverse	GTGGACCACTCGGATGAGCTC
Tnf Forward	CCCTCACACTCAGATCATCTTCT
Tnf Reverse	GCTACGACGTGGGCTACAG
Gzmb Forward	CCACTCTCGACCCTACATGG
Gzmb Reverse	GGCCCCCAAAGTGACATTTATT
Ctla4 Forward	TTTTGTAGCCCTGCTCACTCT
Ctla4 Reverse	CTGAAGGTTGGGTCACCTGTA
Pdcd1 Forward	ACCCTGGTCATTCACTTGGG
Pdcd1 Reverse	CATTTGCTCCCTCTGACACTG
Tigit Forward	CCACAGCAGGCACGATAGATA
Tigit Reverse	CATGCCACCCCAGGTCAAC
Havcr2 Forward	CAAAGCTCCTGAACAGGTAGGG
Havcr2 Reverse	GGTCAGAAATCTCTAGAAAAGCTACCAA
Lag3 Forward	CTGGGACTGCTTTGGGAAG
Lag3 Reverse	GGTTGATGTTGCCAGATAACCC
Ceacam1 Forward	GCCATGCAGCCTCTAACCC
Ceacam1 Reverse	CTGGAGGTTGAGGGTTTGTGC

Table S1.

Primer list for qRT-PCR